Carcinogenesis, 2019, Vol. 40, No. 1, 41–51

doi:10.1093/carcin/bgy170
Advance Access publication November 23, 2018
Original Article

ORIGINAL ARTICLE

Exposure of the extracellular matrix and colonization of the ovary in metastasis of fallopian-tube-derived cancer

Matthew Dean, Vivian Jin, Angela Russo, Daniel D. Lantvit and Joanna E. Burdette*

Department of Medicinal Chemistry and Pharmacognosy, Center for Biomolecular Sciences, University of Illinois at Chicago, Chicago, IL, USA

*To whom correspondence should be addressed. 312-996-6153; Fax: 312-413-9303; Email: joannab@uic.edu

Abstract

High-grade serous ovarian cancer (HGSOC) can originate in the fallopian tube epithelium (FTE), but the role of the ovary in these tumors is unclear. Tumorigenic murine oviductal epithelial (MOE) cells allografted in the ovarian bursa resulted in aggressive tumors that spread throughout the peritoneum whereas intraperitoneal xenografting the same number of cells did not form tumors, indicating that colonization of the ovary may play a role in metastasis. Physical tearing of the ovarian surface to mimic rupture of the ovary during ovulation (independent of hormonal changes) resulted in more MOE and HGSOC cells adhering to the ovary compared with intact ovaries. More MOE cells also adhered to three-dimensional (3D) collagen and primary ovarian stromal cells than to ovarian surface epithelia, indicating that FTE cells adhered to the extracellular matrix exposed during ovulation. However, plating cells on 3D collagen reduced the viability of normal FTE but not cancer cells. Mutation of p53 (R273H or R248W) and activation of Kirsten Rat Sarcoma Viral Oncogene Homolog (KRAS) (G12V) did not increase the viability of MOE cells on 3D collagen. In contrast, loss of phosphatase and tensin homolog (PTEN) allowed MOE cells to retain normal viability on 3D collagen. Loss of PTEN activated AKT and RAC1/c-jun N-terminal kinase signaling that each contributed to the increased viability, invasion and attachment in the collagen rich ovarian microenvironment. These results show that loss of PTEN activates multiple pathways that together enhance colonization of the ovary due to access to 3D collagen, which is a critical organ in the colonization of FTE-derived HGSOC.

Introduction

All epithelial ovarian cancers were thought to originate in the ovarian surface epithelium (OSE), but it is now clear that high-grade serous ovarian cancer (HGSOC) originates from the fallopian tube epithelium (FTE) (1–5). The current model of FTE-derived HGSOC indicates that FTE cells acquire mutations in *Tp53*, resulting in stabilization of the p53 protein (called a p53 signature). Additional mutations result in the formation of serous tubal intraepithelial carcinomas (STICs). STICs metastasize to the ovary, form tumors and then eventually spread throughout the peritoneum (2). However, the role of the ovary in the spread of FTE-derived tumors is unclear (6).

The number of ovulations is associated with a woman's risk of developing HGSOC (7,8). In mice, superovulation increases the formation of ovarian tumors following intrauterine xenograft of tumorigenic cells (9). In primates, OSE cells are lost during ovulation as a stigma forms at the future site of ovulation (10,11), exposing the underlying extracellular matrix (ECM). The ovulatory wound may provide a site for tumorigenic FTE cells to attach to the ovary; however, the role of chemotactic factors produced by the follicle (9,12) and physical disruption of the ovarian surface are difficult to separate *in vivo*.

The only gene ubiquitously mutated in HGSOC is *Tp53* (13), though several different pathway alterations that result in increased PI3K/AKT and extracellular signal-regulated kinase/mitogen-activated protein kinase signaling in serous ovarian cancer have been identified (14). Our laboratory has recently shown that knockdown or knockout of PTEN in the FTE of mice results in FTE-derived ovarian cancer whereas myristoylated AKT (AKT^{myr}) does not (15,16), suggesting that loss of PTEN

Received: May 23, 2018; **Revised:** October 30, 2018; **Accepted:** November 21, 2018

Abbreviations

AKT^{myr}	myristoylated AKT
3D	three dimensional
ECM	extracellular matrix
FTE	fallopian tube epithelium
GFP	green fluorescent protein
HGSOC	high-grade serous ovarian cancer
IB	intrabursal
IP	intraperitoneal
JNK	c-jun N-terminal kinase
MOE	murine oviductal epithelial
MOSE	murine ovarian surface epithelial
MOST	murine ovarian stroma
OSE	ovarian surface epithelium
RFP	red fluorescent protein
RNAseq	RNA sequencing
SCR^{shRNA}	scrambled shRNA
STIC	serous tubal intraepithelial carcinoma

alters signaling in some aspects that differ from AKT activation. The objectives of the current research were to (i) evaluate the role of ovarian colonization in metastases of FTE-derived cells to the peritoneum; (ii) determine if exposure of the ovarian stroma and collagen during ovulation increases colonization by fallopian tube epithelial cells; (iii) identify signaling pathways that allow the FTE to remodel the ovarian ECM and (iv) elucidate the pathways activated by PTEN loss in FTE that are important in colonization of the ovary.

Materials and methods

Cell culture and transfections

Murine oviductal epithelial (MOE) and murine ovarian surface epithelial (MOSE) were originally generated from FVB mice and donated by Barbara Vanderhyden, PhD, University of Ottawa (15). MOE, MOSE, OVCAR3, OVCAR4, OVCAR5, OVCAR8 and OVSAHO cells were maintained in media as described previously (12,17,18). MOE cells stably expressing scrambled shRNA (SCR^{shRNA}), empty vector (NEO), $PTEN^{shRNA}$, AKT^{myr}, $KRAS^{G12V}$ and mutant p53 were previously generated (15,19,20) and were reconfirmed here by reduced PTEN levels, increased phospho-AKT levels, increased phospho-extracellular-signal-regulated kinase or stabilized p53 protein, respectively (Supplementary Figure 1A–E, available at *Carcinogenesis* Online). Production of fluorescent cell lines, transient transfections and treatment with small-molecule inhibitors are described in the Supplementary Materials and Methods, available at *Carcinogenesis* Online. Efficacy of MK2206 (AKT inhibitor), NSC23766 (RAC1 inhibitor) and c-jun N-terminal kinase (JNK) inhibitor VIII (JNK inhibitor) was validated in MOE cells by treating the cells with a dose response of each inhibitor for 24 h and measuring phospho-AKT, phospho-JNK and phospho-cJun, respectively, via western blot (Supplementary Figure 1F–H, available at *Carcinogenesis* Online).

Allograft experiment and immunohistochemistry

All animal procedures were approved by the Institution Animal Care and Use Committee and complied with the *Guide for the Care and Use of Laboratory Animals*. MOE $KRAS^{G12V}$ + $PTEN^{shRNA}$ cells (50 000 in phosphate-buffered saline) were injected into the peritoneum [intraperitoneal (IP)] or ovarian bursa [intrabursal (IB)] of 8-week-old female athymic nu/nu mice (Taconic, Germantown, NY). The health of mice was monitored daily, and mice were killed at humane end points. At necropsy, the peritoneal space was visually inspected for ascites and tumors, which were fixed in 4% paraformaldehyde overnight, dehydrated in ethanol and embedded in paraffin. Immunochemistry (Supplementary Table 2, available at *Carcinogenesis* Online) was carried out as described previously (15).

Ex vivo adhesion assay

An assay to measure adhesion of fluorescently tagged cells to murine ovaries has been recently described (16). Ovaries were removed from CD-1 mice between days 16 and 18. Ovaries were left intact or the surface was disrupted with a scalpel blade to mimic ovulation. Each ovary was placed in a 1.8 ml microfuge tube with 1 ml of media and 30 000 cells labeled with green fluorescent protein (GFP) or red fluorescent protein (RFP). Tubes were incubated on an orbital shaker for 24 h at 37°C at 40 r.p.m. Ovaries were washed 2× in phosphate-buffered saline to remove non-adhered cells, and ovaries were inspected with a Nikon Eclipse TS100 inverted microscope. The number of fluorescent cells attached to the ovary was counted on both sides and averaged. A representative fluorescent and bright field image was taken, and the fluorescent pixels were pasted on top of the bright field image using ImageJ (imagej.nih.gov) to produce the overlay image.

Collagen treatment, migration assay and invasion assays

Production of conditioned media, scratch assays to measure migration and Boyden chamber invasion assays were done according to well-established protocols. Collagen was added to wells as a two-dimensional (2D) or three-dimensional (3D) layer as described previously (21). A complete description is available in the Supplementary Materials and Methods, available at *Carcinogenesis* Online.

Adhesion assays

Isolation and growth of the murine ovarian stroma (MOST) cells is described in the Supplementary Materials and Methods, available at *Carcinogenesis* Online. MOE GFP cells (100 000) were added to wells with a confluent monolayer of MOST, a monolayer of MOSE or a 3D collagen gel and incubated for 2 h. Washed monolayers were imaged with an inverted fluorescent microscope, and fluorescence was measured with a BioTek Synergy Plate Reader. Adhesion to fibronectin, vitronectin, laminin, collagen and collagen IV was measured with the Millicoat ECM Screening Kit (ECM205; Millipore, Billerica, MA) per the manufacturer's instructions.

To determine if MOE cells adhere on top of or in between MOSE cells, MOSE cells were seeded at indicated concentrations on 96-well plates pretreated with 2D type I collagen. The next day, media were removed, and the cells were stained with CellTracker Red DMPTX dye (C34552; Life Technologies, Waltham, MA). Next, 100 000 MOE GFP cells were seeded into each well. After 2 h, images were captured with a 4× objective. Subsequently, the media were removed from each well, the cells were rinsed with phosphate-buffered saline and 100 µl lysis buffer was added to each well. The plates were frozen at –80°C, thawed and 80 µl lysis buffer was transferred to white 96-well plates (3789; Corning, Corning, NY). The relative number of MOE cells in each well was determined by measuring fluorescence intensity of GFP with the BioTek Synergy Plate Reader.

Viability assay

Cells (20 000–50 000 dependent on cell line) were plated on 2D collagen or 3D collagen in a 96-well plate in 100 µl media and cultured for 24 h. Viability was measured with CellTiter-Glo Luminescent Cell Viability Kit (G7570; Promega) per the manufacturer's instructions. Results are expressed as the ratio of viability of the same cell line or treatment on 3D collagen to viability on 2D collagen (3D:2D viability ratio).

RNA isolation, qPCR, RNAseq and western blot

RNA isolation, quantitative PCR, RNA sequencing (RNAseq) and western blots were carried out as described previously (12,15,18). A detailed description of these methods is available in the Supplementary Materials and Methods available at *Carcinogenesis* Online.

Statistical analysis

All data are presented as mean ± SEM and n = 3–5. Data were analyzed by a one-sample t-test compared to 1, a two-sample *t*-test or an analysis of variance (ANOVA) followed by a Dunnett's or Tukey's *post hoc* test,

depending on the hypothesis and number of treatments. Data were analyzed with Prism, version 7.0a (www.graphpad.com). Significance was defined at $P < 0.05$.

Results

Colonization of the ovary is important for peritoneal metastasis of FTE-derived tumors

Previous evidence suggested that ovarian cancer cells preferentially colonized the ovary, an event facilitated by ovulation (9,22). We demonstrated that MOE KRAS^{G12V} + PTEN^{shRNA} cells were tumorigenic after intraperitoneal (IP) xenograft of 10 million cells (15). To determine if MOE KRAS^{G12V} + PTEN^{shRNA} could form tumors after intrabursal (IB) xenograft, which limits the xenograft to a small volume, 50 000 MOE KRAS^{G12V} + PTEN^{shRNA} cells were allografted into the right and left bursa of two mice. Mice developed aggressive tumors, requiring killing on days 64 and 97. Tumors were observed in every peritoneal organ examined (Supplementary Figure 2A, available at *Carcinogenesis* Online). Next, to evaluate the role of ovarian colonization in metastasis of FTE-derived cancer cells, 50 000 MOE KRAS^{G12V} + PTEN^{shRNA} cells were allografted into the left ovarian bursa (unilateral IB) in three mice. To mimic what would happen if an equal number of cells exfoliated from the fallopian tube, but were not directly interacting with the ovary, 50 000 cells were xenografted intraperitoneally into five mice. No tumors were observed in any of the IP-injected mice for the duration of the experiments (150 days; Figure 1A). One IP mouse was killed on day 123 for unrelated health reasons, but no tumors were observed (Supplementary Figure 2B, available at *Carcinogenesis* Online). All unilateral IB allografted mice developed tumors, necessitating killing due to tumor burden by day 90 ($P < 0.05$). All unilateral IB mice (3/3) developed tumors in the gastrointestinal tract, omentum, pancreas, reproductive tract and ascites, and two-thirds of mice had tumors in the diaphragm (Figure 1B and C). In unilateral IB-injected mice, the left ovary was on average 16.5 mm in diameter compared with 5.84 mm for the right ovary ($P < 0.0001$) due to tumor burden, and both ovaries in unilateral IB-injected mice were larger than ovaries of IP mice (2.65 mm; $P < 0.05$; Figure 1D–E).

In unilateral IB-injected mice, the ipsilateral ovary was completely degraded by tumor cells as evidenced by the absence of observable follicles or corpus lutea , and tumors had pockets of necrotic tissue with a lack of nuclear staining. Immunostaining

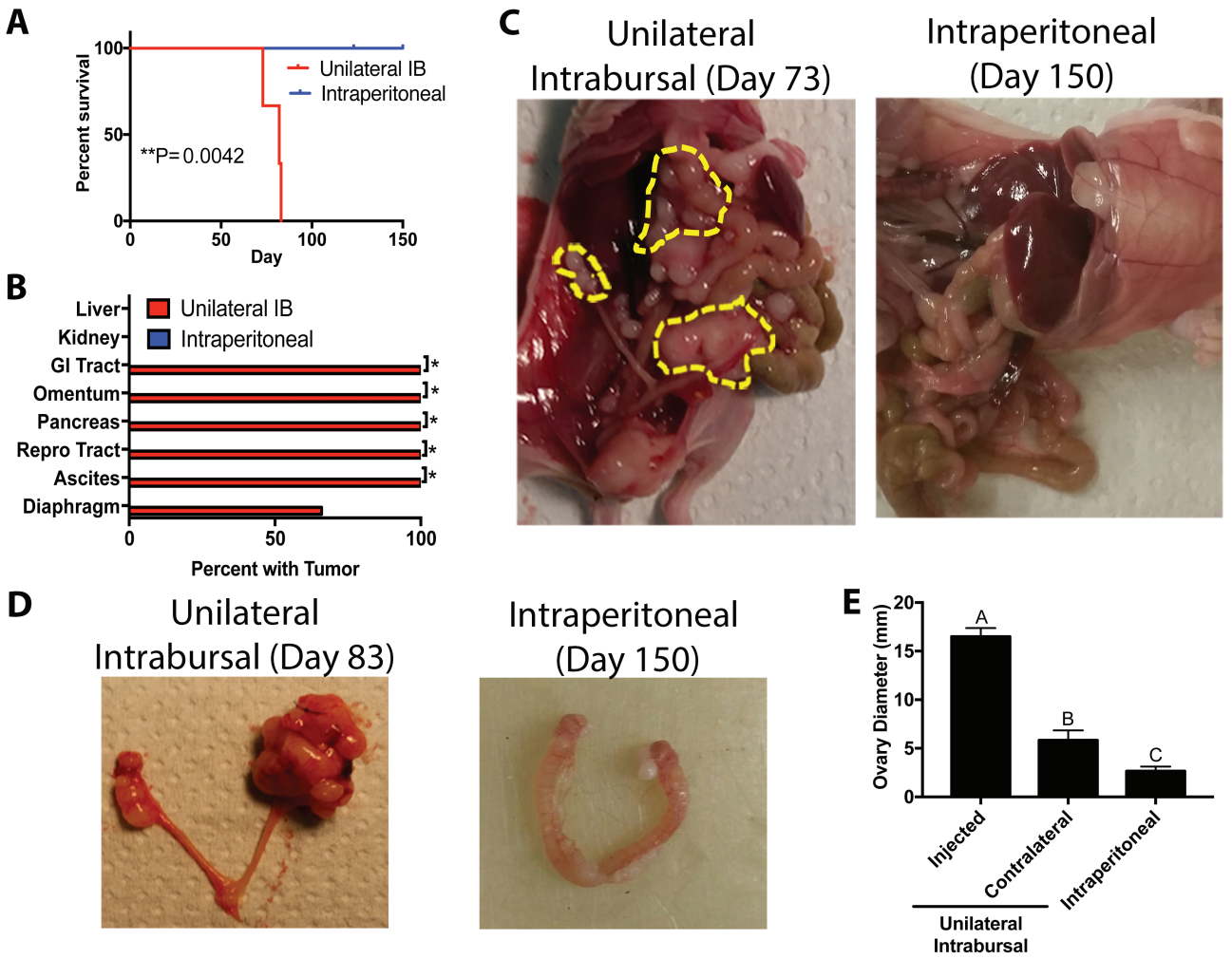

Figure 1. Colonization of the ovary is an important step in metastasis of FTE-derived cancer cells. (**A**) Kaplan–Meier analysis of mice following xenograft of MOE KRAS^{G12V} + PTEN^{shRNA} cells into the left bursa (unilateral IB) or IP. (**B**) Distribution of visible tumors in the peritoneum after unilateral IB and IP xenografts. (**C** and **D**) Representative images of mice and reproductive tracts from unilateral IB and IP xenografts. (**E**) Diameter of ovaries in unilateral IB and IP xenografts mice ($n = 3–5$). Bars without common letter differ, $^{A–C}P < 0.05$. Significantly different from unilateral IB, $^{*}P < 0.05$.

for PAX8, a marker of the FTE, was widespread in the left ovary, confirming that tumor cells were derived from the FTE. Tumors from MOE $KRAS^{G12V}$ + $PTEN^{shRNA}$ tumors were highly proliferative and had widespread Ki67 staining. Tumor tissue and some follicles and corpus lutea in the contralateral ovaries had high Ki67 immunostaining. No evidence of ovarian colonization was found in the IP-injected mice, with defined follicles and corpus luteum in the hematoxylin and eosin sections. PAX8 immunostaining was negative and Ki67 immunostaining was low (Supplementary Figure 3, available at *Carcinogenesis* Online).

Exposure of ovarian collagen increases attachment to the ovary

The individual contributions of hormones and physical tearing of the ovary during ovulation on tumor cell colonization are difficult to separate *in vivo*. Therefore, an *ex vivo* adhesion assay was used to isolate and test the role of physical rupture of the ovary, which would expose underlying 3D collagen, on attachment of FTE cells (16). Murine ovaries were either left intact or the surface was ruptured with a scalpel to mimic ovulation independent of hormonal changes. The wound resulted in loss of the OSE and disruption of the ovarian surface (hematoxylin and eosin images in Supplementary Figure 4A–B, available at *Carcinogenesis* Online) (11). Intact and ovulation mimetic treated ovaries were incubated with MOE GFP cells for 24 h on an orbital shaker. Ovulation mimetic increased the number of MOE GFP cells adhering to the surface of each ovary by 3.2-fold ($P < 0.01$; Figure 2A and B). Similarly, the ovulation mimetic increased attachment of HGSOC cell lines, OVCAR8 RFP and OVCAR4 RFP cells (2.5- and 1.7-fold increase, respectively; $P < 0.05$; Figure 2C and D and Supplementary Figure 4C, available at *Carcinogenesis* Online). Next, MOE $PTEN^{shRNA}$ cells were incubated with ovulation mimetic ovaries followed by immunohistochemistry to determine where MOE cells were adhering. PAX8 immunostaining was clearly observed at the wounded surface (Supplementary Figure 4D, available at *Carcinogenesis* Online) with sporadic PAX8 staining on the intact OSE-lined surfaces of the ovary. Numerous MOE $PTEN^{shRNA}$ cells were also observed attached at the hilus region (Supplementary Figure 4E, available at *Carcinogenesis* Online), suggesting that the MOE cells are preferentially adhered to any area where the ovarian surface is disrupted. To confirm that the effect of ovulation mimic was not due to the increased secretion of chemotactic factors leaking out after wounding, conditioned media were produced using intact and ovulation mimetic ovaries. Conditioned media from intact and wounded ovaries equally increased migration of MOE cells (P– = 0.96) by approximately 3-fold ($P < 0.01$) (Supplementary Figure 4F, available at *Carcinogenesis* Online). These data confirmed that the ovulation mimetic model did not increase the release of chemotactic factors by the ovary.

To determine if cells were adhering to ovulation mimetic ovaries due to exposure of the ECM, MOE GFP cells were plated on monolayers of MOSE cells to model the intact ovarian surface, which is covered with a single layer of ovarian surface cells. MOE GFP cells were also plated onto monolayers of MOST cells to mimic rupture sites within the ovary (Supplementary Figure 5A, available at *Carcinogenesis* Online). Lastly, MOE GFP were plated onto 3D type I collagen gels, because this is the primary ECM in the ovarian stroma (Supplementary Figure 5B, available at *Carcinogenesis* Online). As predicted, 6.7× more MOE GFP cells bound to MOST relative to MOSE monolayers ($P < 0.05$). Supporting a role for collagen as a binding surface for metastatic FTE-derived HGSOCs, 3-fold more cells bound to 3D collagen gel relative to MOST cells ($P < 0.0001$; Figure 2E and F). In a 2D adhesion assay, MOE cells bound equally well to type I collagen (primarily a stromal ECM protein), type IV collagen and laminin, which are all primarily basement membrane ECM proteins. About 25% less MOE cells bound to vitronectin, a glycoprotein found in high concentrations in serum (Figure 2G; $P < 0.05$). Finally, the ability of OSE cells to hinder binding to underlying type I collagen was tested by plating an increasing number of MOSE cells on top of 2D type I collagen in a 96-well plate and then performing adhesion assays with MOE GFP cells. Increasing the number of MOSE cells in each well led to a linear decrease in MOE GFP attachment ($P < 0.0001$, $R^2 = 0.9047$; Figure 2H). Staining the MOSE monolayer with CellTracker Red dye showed that in subconfluent wells, MOE GFP adhered between MOSE cells. In confluent wells, MOE GFP adhered between MOSE cells when possible, but some MOE GFP cells did adhere on top of the MOSE monolayer (Figure 2I). These results suggest that FTE preferentially adhere to ECM proteins (including type I collagen) that are under the ovarian surface and are exposed during ovulation (10,11).

Loss of PTEN increases the ability of FTE cells to grow on 3D type I collagen

RNAseq was used to compare the transcriptome of MOE cells grown on 2D or 3D collagen. The time period of adhesion to 3D collagen was optimized by monitoring connective tissue growth factor (*CTGF*) expression, which decreased after 6 h ($P < 0.05$; Supplementary Figure 5C, available at *Carcinogenesis* Online) (21). RNAseq-identified 847 transcripts decreased (including *CTGF*) and 692 transcripts increased by 3D collagen (Supplementary Figure 5D, available at *Carcinogenesis* Online; GSE112397). Interestingly, Kyoto Encyclopedia of Genes and Genomes (KEGG) analysis of transcripts that were downregulated by 3D collagen identified pathways regulating focal adhesion, actin cytoskeleton and ECM–receptor interaction (Figure 3A), suggesting that untransformed MOE cells may respond poorly to a microenvironment rich in 3D collagen. Next, we measured the viability of a panel of normal and HGSOC cell lines 24 h after plating on 2D and 3D collagen. To account for intrinsic differences in the viability of different cell lines, viability of each cell line on 3D collagen was normalized to the viability of the same cell line on 2D collagen (3D:2D viability ratio). The 3D:2D viability ratio of three normal cell lines (MOE, MOSE and IOSE80) was reduced on 3D collagen relative to their viability on 2D collagen (3D:2D viability ratio <1; $P < 0.05$). In contrast, the viability of all four HGSOC cell lines (OVCAR3, OVCAR4, OVCAR8 and OVSAHO) was unaffected by 3D collagen (3D:2D viability ratio = 1; Figure 3B, morphology on plastic, 2D collagen and 3D collagen shown in Supplementary Figures 6 and 7, available at *Carcinogenesis* Online). These data indicate that even though normal FTE attached to the collagen exposed by ovulation, HGSOC lines are better at surviving in a microenvironment rich in 3D type I collagen than normal epithelial cells.

KEGG analysis of transcripts increased in response to growth on 3D collagen found significant differences in the p53 pathway (Figure 3C). Analysis of the data found that the KEGG pathway identified only six transcripts associated with p53 signaling that were significantly altered (Supplementary Figure 8A, available at *Carcinogenesis* Online). Therefore, the list of genes altered by 3D collagen was compared with a list of canonical p53 targets (23). Of the 41 well-established canonical p53 targets identified by Nikulenkov *et al.*, only 17% were significantly different in the RNAseq dataset (Supplementary Figure 8B, available at *Carcinogenesis* Online). In addition, plating MOE cells on 2D or 3D

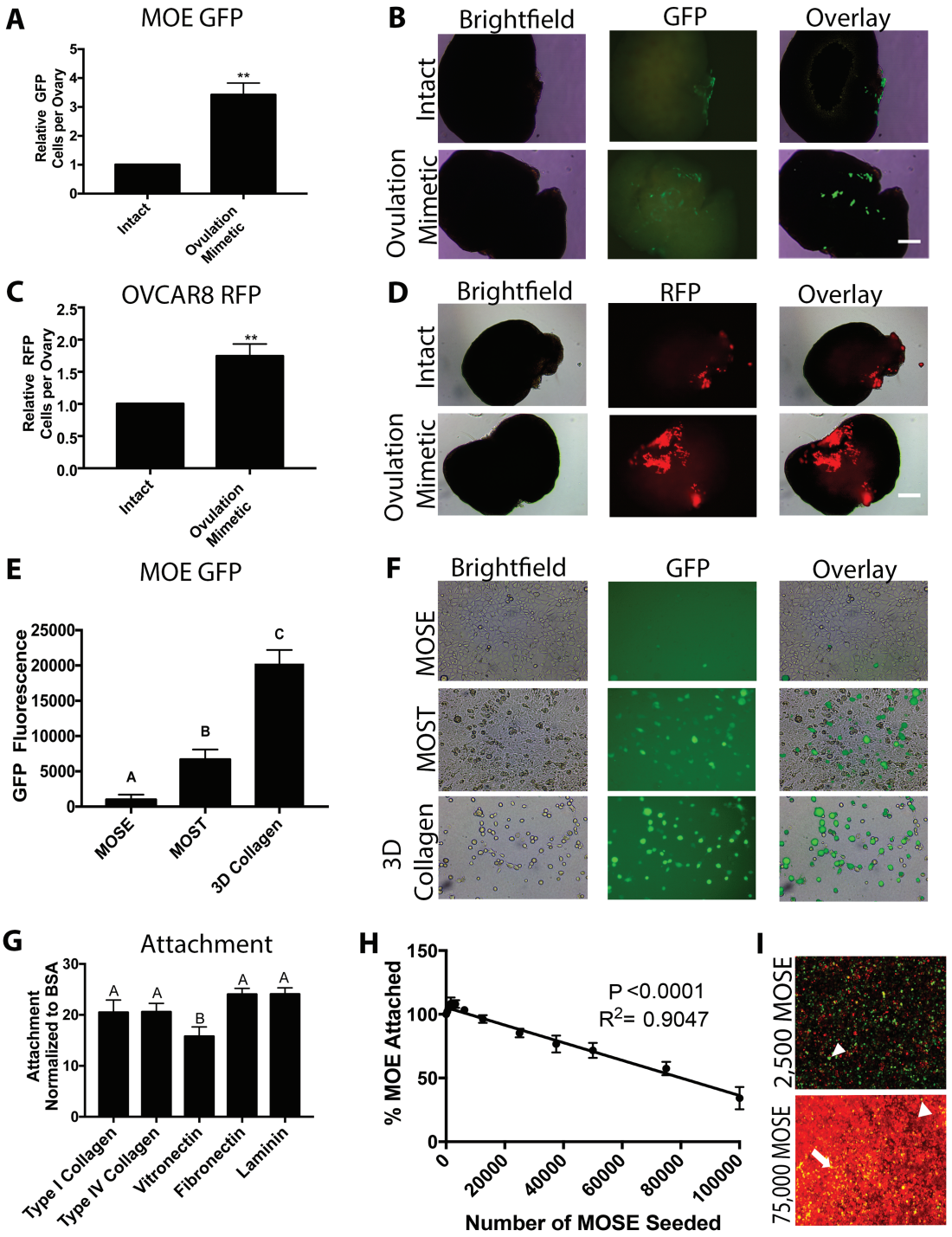

Figure 2. Mimicking ovulation by wounding the ovary increases attachment of FTE cells. (**A–D**) Rupture of the ovarian surface (ovulation mimetic) increases attachment of MOE GFP (equivalent to fallopian tube) (A, B) and OVCAR8 RFP (C, D) to the *ex vivo* cultured murine ovaries. (**E** and **F**) Attachment of MOE GFP cells to a monolayer of MOSE , monolayer of MOST or 3D type I collagen gels. (**G**) Attachment of MOE cells to five ECM proteins present in the basement membrane and stroma. (**H** and **I**) Attachment of MOE GFP to 2D type I collagen in wells with increasing number of MOSE cells labeled with CellTracker Red dye (arrowhead = MOE GFP attached to plastic; arrow = MOE GFP cell attached on top of MOSE). n = 3–5. Scale bar = 100 μm. Significantly different from intact, $^{**}P < 0.01$. Bars without common letter differ, $^{A–C}P < 0.05$. BSA, bovine serum albumin.

collagen for 24 h did not result in stabilization of the p53 protein based on western blots (Supplementary Figure 8C, available at *Carcinogenesis* Online). Functionally, the viability of MOE cells expressing the two most common mutations in p53 (R273 and R248) was reduced on 3D collagen to a similar extent (20–30%) as the vector control cells (Supplementary Figure 8D, available at *Carcinogenesis* Online). These data indicate that mutation in p53 was not sufficient to allow cells to thrive in a microenvironment rich in 3D collagen.

In HGSOC, alterations that activate PI3K/AKT and mitogen-activated protein kinase/extracelluar regulated kinase are common, and these pathways are well known to regulate cell

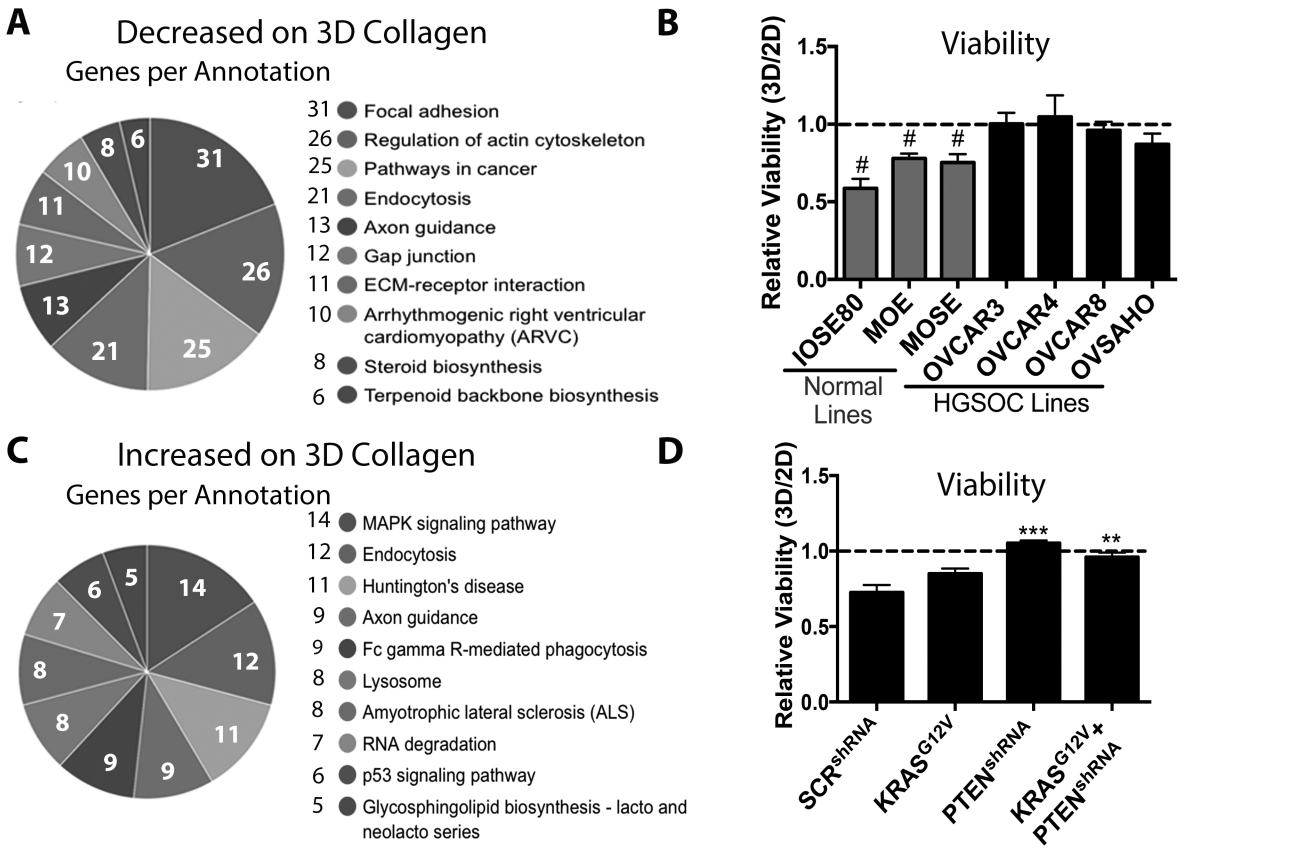

Figure 3. Loss of PTEN allows FTE cells to survive in a collagen-rich microenvironment. (**A**) KEGG analysis of genes decreased by culture on 3D collagen for 6 h. (**B**) 3D:2D viability ratio of normal (IOSE80, MOE and MOSE) and HGSOC cells (OVCAR3, OVCAR4, OVCAR8 and OVSAHO). (**C**) KEGG analysis of genes increased by culture on 3D collagen. (**D**) 3D:2D viability ratio of MOE cells stably expressing a control vector, $KRAS^{G12V}$, $PTEN^{shRNA}$ or $KRAS^{G12V}$ + $PTEN^{shRNA}$. (**E**) Representative western blots for phospho-AKT, AKT and β actin of MOE cells treated with 100 ng/ml of collagen for indicated time points. (**F**) Representative western blot for MOE cells plated on 2D collagen for indicated times. (**G**) Representative western blots for phospho-AKT, AKT and β actin of MOE cells cultured on plastic, 2D collagen and 3D collagen for 24 h. Data are plotted as mean ± SEM (n = 3–5). Significantly different from 1, #$P < 0.05$. Significantly different from control, **$P < 0.01$, ***$P < 0.001$.

viability and survival in many other contexts (24,25). Therefore, we tested the viability of MOE cells stably expressing $KRAS^{G12V}$, $PTEN^{shRNA}$ or $KRAS^{G12V}$ + $PTEN^{shRNA}$. MOE $KRAS^{G12V}$ cells showed a slightly better 3D:2D viability ratio as compared with normal cells, but this did not reach statistical significance (P = 0.088; Figure 3D). In contrast, stable expression of $PTEN^{shRNA}$ completely rescued the 3D:2D viability ratio of MOE cells. The 3D:2D viability ratio of MOE $KRAS^{G12V}$+ $PTEN^{shRNA}$ was similar to that of MOE $PTEN^{shRNA}$ alone (Figure 3D), indicating that $PTEN^{shRNA}$, by itself, is sufficient to rescue the relative viability of MOE cells on 3D collagen.

Given that collagen is well known to activate PI3K/AKT signaling in other cell types (26,27), we tested the ability of collagen to increase phospho-AKT in MOE cells by western blot. Because of the transient nature of AKT phosphorylation in response to extracellular stimulation and the time required for cells to attach to collagen after plating (~1–2 h), we added 100 ng/ml collagen to the media of MOE cells that were grown on plastic and serum-starved for 24 h. Treatment with collagen resulted in a dramatic increase in phospho-AKT levels at 60 min, which returned to baseline at 120 and 240 min (Figure 3E). Plating MOE cells on 2D collagen led to an increase in phospho-AKT at 1 h that was absent by 2 and 3 h (Figure 3F), confirming a transient increase in AKT activation. To investigate prolonged phospho-AKT activation due to collagen, MOE cells were plated on plastic, 2D collagen and 3D collagen for 24 h, and no differences in phospho-AKT levels were detected (Figure 3G). These results suggest that sustained

activation of PI3K signaling enhances MOE cellular survival in a microenvironment rich in 3D collagen.

Colonization of the ovary is a complex process. In addition to just surviving in a 3D collagen-rich microenvironment, cells must first attach to the ovary and then invade. Therefore, the ability of MOE cells stably expressing $KRAS^{G12V}$ or $PTEN^{shRNA}$ to attach to type I collagen was further characterized. The ability of MOE cells stably expressing a scrambled shRNA (SCR^{shRNA}) with RFP and MOE $PTEN^{shRNA}$ RFP cells to adhere to murine ovaries was measured. MOE $PTEN^{shRNA}$ RFP cells attached 3-fold more to ovulation mimetic ovaries than MOE SCR^{shRNA} RFP ($P < 0.001$; Figure 4A and B). Expression of $KRAS^{G12V}$, $PTEN^{shRNA}$ and $KRAS^{G12V}$+$PTEN^{shRNA}$ significantly increased invasion of MOE cells thorough collagen (1.7- to 2.6-fold over MOE SCR^{shRNA}; $P < 0.05$; Figure 4C and D). After 7 days on 3D collagen, the relative viability of $KRAS^{G12V}$ + $PTEN^{shRNA}$ was higher than that of control cells, $KRAS^{G12V}$ cells and $PTEN^{shRNA}$ cells (Figure 4E), suggesting that the combination was necessary for long-term viability on 3D collagen. Surprisingly, MOE $PTEN^{shRNA}$ and $KRAS^{G12V}$ + $PTEN^{shRNA}$ cells formed spheroids in 3D collagen (Figure 4F), similar to the spheroids formed by OVCAR8 cells (Figure 4G). MOE $KRAS^{G12V}$ cells formed spheroid-like structures, but they did not exhibit the typical smooth, spherical morphology. These results indicate that silencing PTEN increases the ability of FTE cells to attach to ovaries and invade, survive and form spheroids in a type I collagen-rich microenvironment.

AKT and RAC1/JNK mediates the effects of $PTEN^{shRNA}$ in FTE cells

AKT activation occurs after PTEN loss (Supplementary Figure 9A, available at *Carcinogenesis* Online); therefore, the role

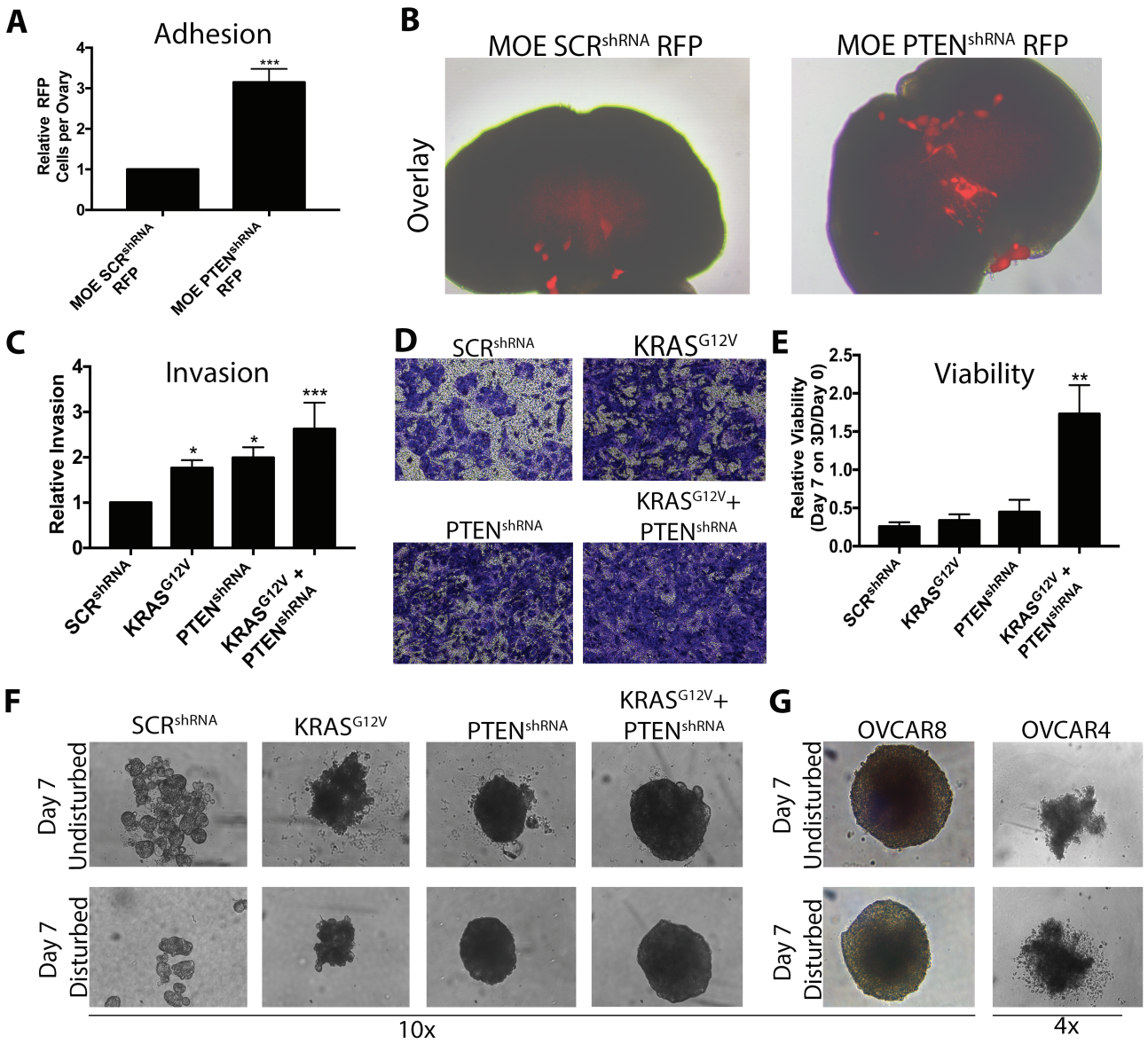

Figure 4. Loss of PTEN increases the ability of FTE cells to adhere, invade and form spheroids in 3D collagen. (**A** and **B**) Attachment of MOE SCR^{shRNA} RFP and MOE $PTEN^{shRNA}$ RFP cells to ovulation mimetic ovaries. (**C** and D) Boyden chamber invasion through 3D collagen of MOE cells stably expressing SCR^{shRNA} (control), $PTEN^{shRNA}$, $KRAS^{G12V}$ or $KRAS^{G12V}$ + $PTEN^{shRNA}$. (**E**) Viability of MOE cell lines plated on 3D collagen for 7 days. (**F** and **G**) Representative images of structures formed by MOE cell lines (F) or HGSOC lines (G) after 7 days. (F) Data are plotted as mean ± SEM (n = 3–5). Significantly different from MOE SCR^{shRNA}, *$P < 0.05$, **$P < 0.01$, ***$P < 0.001$.

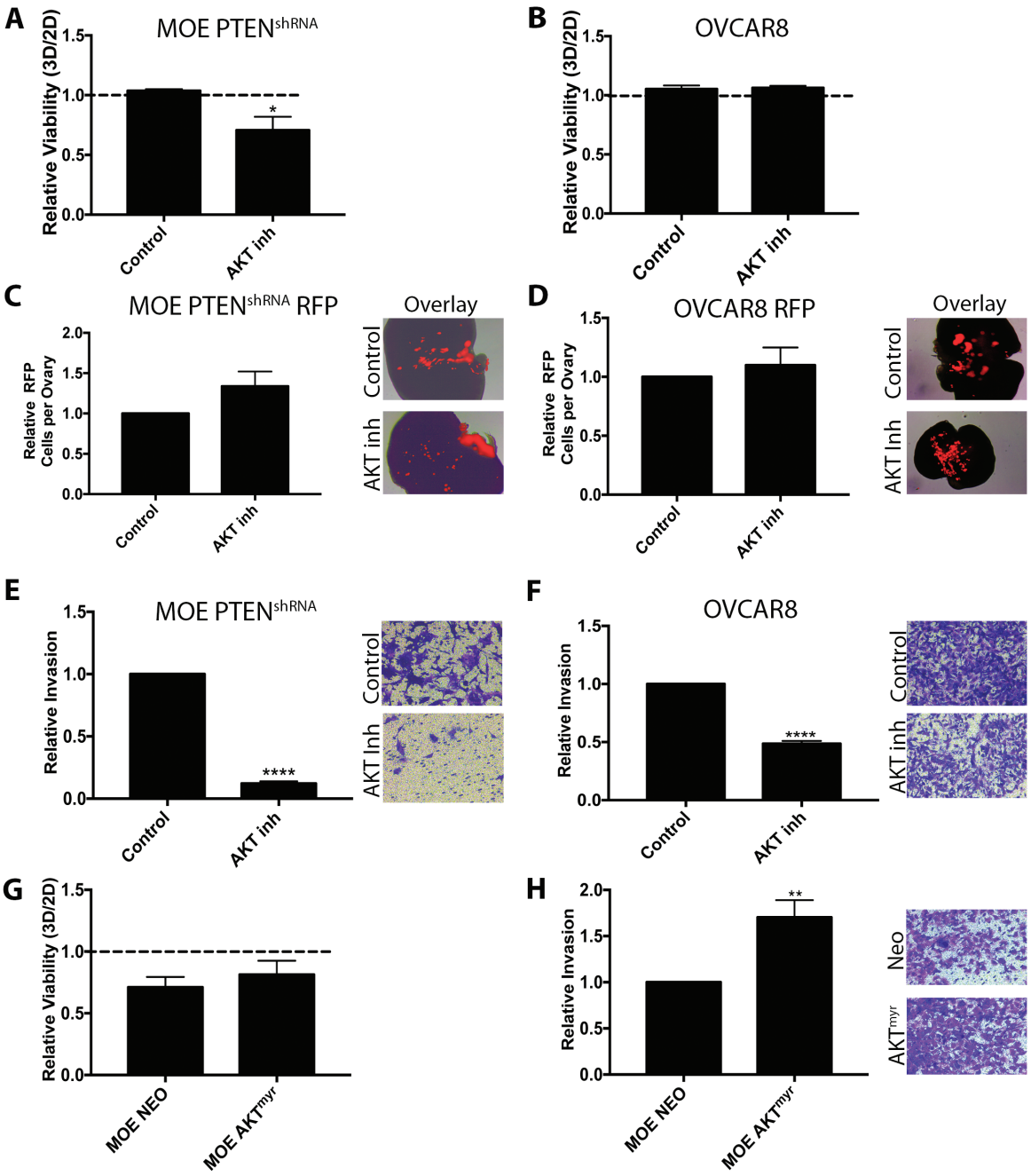

Figure 5. AKT is sufficient to increase invasion, required but not sufficient to increase viability and does not mediate increased ovarian attachment of MOE cells. (**A** and **B**) Viability ratio of MOE PTEN^{shRNA} (A) and OVCAR8 (B) cells cultured on 2D or 3D collagen with the AKT inhibitor (MK2206) or DMSO (control). (**C** and **D**) Attachment of MOE PTEN^{shRNA} RFP (C) and OVCAR8 RFP (D) cells to ovulation mimetic ovaries in the presence of dimethyl sulfoxide (DMSO) (control) or MK2206. (**E** and **F**) Boyden invasion assays through 3D collagen in the presence of DMSO (control) or MK2206. (**G**) 3D:2D viability ratio of control (MOE NEO) and MOE AKT^{myr} cells. (**H**) Invasion of MOE NEO and MOE AKT^{myr} through 3D collagen in Boyden assays. Data are plotted as mean ± SEM (n = 3–5). Significantly different from control or MOE NEO, *$P < 0.05$, **$P < 0.01$, ****$P < 0.0001$.

of AKT in mediating the phenotypes seen in MOE PTEN^{shRNA} cells was assessed using the AKT inhibitor MK2206. MK2206 (10 μM) reduced the 3D:2D viability ratio of MOE PTEN^{shRNA} from 1.05 to 0.71 ($P < 0.05$; Figure 5A). However, MK2206 had no effect on the 3D:2D viability ratio of OVCAR8 cells (Figure 5B). Interestingly, MK2206 had no effect on the attachment of either MOE PTEN^{shRNA} RFP or OVCAR8 RFP cells to ovulation mimetic ovaries (Figure 5C and D), suggesting this effect of PTEN^{shRNA} is not entirely dependent on AKT alone. MK2206 dramatically reduced invasion of MOE PTEN^{shRNA} cells through collagen by 87% ($P < 0.0001$; Figure 5E) and invasion of OVCAR8 cells through collagen by 52% ($P < 0.0001$; Figure 5F). To determine if activation of AKT could similarly increase viability and invasion observed with MOE PTEN^{shRNA} cells, the MOE AKT^{myr} cells were investigated. Stable expression of AKT^{myr} in MOE cells increased phospho-AKT to a similar extent as PTEN^{shRNA} (Supplementary Figures 1C and 8A, available at *Carcinogenesis* Online). However, AKT^{myr} did not rescue the viability ratio of MOE cells (Figure 5G). AKT^{myr} increased invasion of MOE cells (1.7-fold, $P < 0.01$; Figure 5H), though the effect was 30% less than seen in the MOE PTEN^{shRNA}

cells. These data indicate that phospho-AKT only partially mediates the effects seen in MOE PTEN^{shRNA} cells and support recent reports from other tumor types that transformation following PTEN loss or PI3K activation increases signaling via multiple pathways (25,26,28).

In other cell types, loss of PTEN activates RAC1 and JNK signaling (29–31), and recently we demonstrated that RAC1 stimulated activin A-induced migration of MOE cells (12). Western blots indicated higher phosphorylation levels of the p54 splice variant of JNK in MOE PTEN^{shRNA} relative to MOE SCR^{shRNA} ($P < 0.01$), but no difference in phosphorylation level of the p46 splice variant (Figure 6A). To interrogate the role of RAC1 and JNK, we used the small molecule inhibitors NSC23766 and JNK inhibitor V, respectively. Confirming that RAC1 mediates the increase in phospho-JNK, NSC2766 significantly reduced phospho-JNK levels in MOE PTEN^{shRNA} cells ($P < 0.05$; Figure 6B). Phospho-JNK levels were not altered in MOE AKT^{myr} relative to MOE NEO (Supplementary Figure 9B, available at *Carcinogenesis* Online), confirming that PTEN^{shRNA}-induced activation of RAC1/JNK signaling is not dependent on phospho-AKT. Neither the RAC1 nor the JNK inhibitor reduced the 3D:2D viability ratio of MOE PTEN^{shRNA} or OVCAR8 cells (Supplementary Figure 9C–D, available at *Carcinogenesis* Online). Both inhibitors, however, reduced attachment of MOE PTEN^{shRNA} RFP cells to ovulation mimetic ovaries by 40% ($P < 0.0001$; Figure 6C). These inhibitors were more effective in OVCAR8 RFP cells, reducing *ex vivo* adhesion by ~75% ($P < 0.01$; Figure 6D). In confirmation, a RAC1^{siRNA} (previously validated (12)) reduced adhesion of MOE PTEN^{shRNA} RFP by approximately 40% ($P < 0.05$; Supplementary Figure 9E, available at *Carcinogenesis* Online). Inhibition of RAC1 and JNK also reduced invasion of MOE PTEN^{shRNA} through 3D collagen gels by 40% ($P < 0.01$; Figure 6E) and invasion of OVCAR8 cells by >30% ($P < 0.05$; Figure 6F). The guanine exchange factors PREX1 and PREX2 activate RAC1 after loss of PTEN in breast cancer (31). As PREX1 was undetectable in our RNAseq dataset, we tested the ability of a PREX2^{siRNA} to reduce ovarian adhesion of MOE PTEN^{shRNA} RFP cells to murine ovaries. The PREX2^{siRNA} dramatically reduced PREX2 protein levels over 3 days

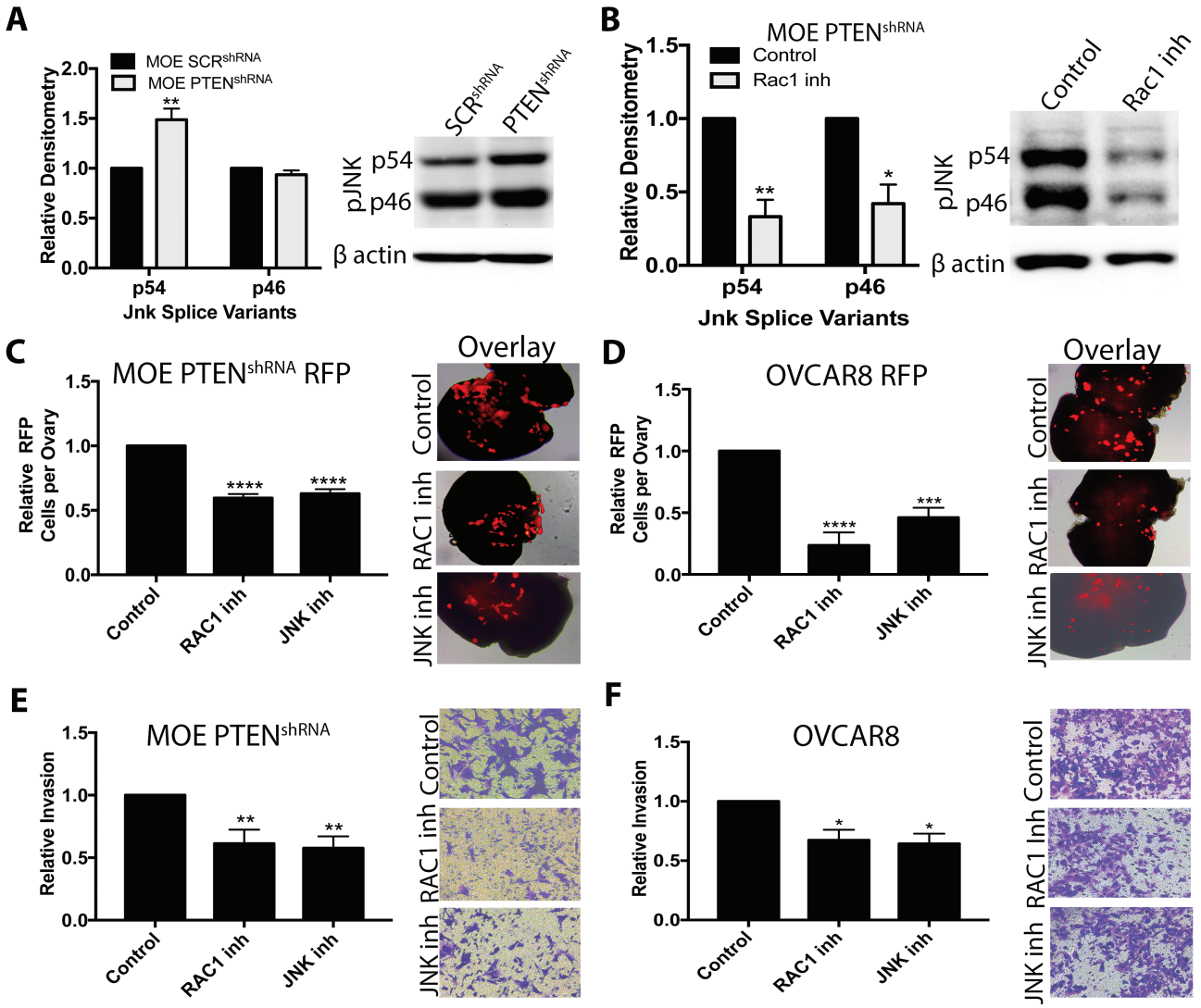

Figure 6. RAC1/JNK signaling mediates the effects of PTEN loss on ovarian adhesion and migration through 3D collagen. (**A** and **B**) Representative western blots for phospho-JNK and β actin in MOE SCR^{shRNA} and MOE PTEN^{shRNA} cells (A) and MOE PTEN^{shRNA} cells treated with a RAC1 inhibitor (NSC23766). (**C** and **D**) Adhesion of MOE PTEN^{shRNA} RFP cells (C) and OVCAR8 RFP (D) to ovulation mimetic ovaries in the presence of vehicle (control), a RAC1 inhibitor or a JNK inhibitor (JNK inhibitor VIII). (**E** and **F**) Invasion through type I collagen of MOE PTEN^{shRNA} (E) and OVCAR8 cells (F). Data are plotted as mean ± SEM ($n = 3–5$). Significantly different from control or MOE SCR^{shRNA}, *$P < 0.05$, **$P < 0.01$, ***$P < 0.001$, ****$P < 0.0001$.

(Supplementary Figure 9F–G, available at *Carcinogenesis* Online) but had no effect on ovarian adhesion of MOE PTEN^{shRNA} RFP cells (Supplementary Figure 9H, available at *Carcinogenesis* Online). Collectively, these results indicate that RAC1/JNK contributes to the effects of PTEN^{shRNA} in MOE cells.

Discussion

The current results suggest that colonization of the ovary may represent an important step in peritoneal metastasis of FTE-derived cancer. A mere 50 000 MOE KRAS^{G12V} + PTEN^{shRNA} cells injected into the ovarian bursa developed into aggressive tumors that spread throughout the peritoneum and resulted in death of the animals, whereas peritoneal grafting with this number of cells did not result in a single tumor forming. In a previous study, IP xenograft of 1×10^7 of the same cells resulted in tumor formation (15), with mice succumbing to the disease in a similar time frame as in this study. IB allografting results in a higher density of tumorigenic cells due to the confined nature of this membrane-encapsulated space. One theory could be that tumorigenic cells would be in higher concentration near the ovary as they are exfoliated from STIC lesions in the fallopian tube and dispersed into the peritoneal space. We hypothesize that the ovary represents a unique organ for primary metastasis in part due to its proximity to the fallopian tube. Previous studies confirmed that xenografting HGSOC cancer cells, but not other types of cancer cells, intravenously resulted in tumor formation in the ovary (22). In a transgenic mouse model (*Brca*, *Tp53*, *Pten*), ovariectomy reduced peritoneal metastasis, further demonstrating the importance of the ovary in peritoneal spread (32). Collectively, these data suggest that colonization of the ovary is a key step in metastasis of FTE-derived tumors and that understanding the mechanisms that drive tumorigenic FTE cells to colonize the ovary may improve strategies to disrupt this step and increase survival.

Physically cutting the ovarian surface was used in this study to mimic physical rupture of the ovary during ovulation, which might change the ovarian microenvironment in ways other than simply exposing the underlying ECM. However, conditioned media from intact and ovulation mimetic ovaries equally stimulated migration of MOE cells, indicating that alterations in adhesion were likely not due to chemotactic factors leaking out of the ovary after cutting in our experiments using ovulation mimetic ovaries. MOE cells attached to type I collagen and MOST cells better than to MOSE and increasing the number of MOSE cells hindered adhesion of MOE GFP cells to the underlying collagen. Yang-Hartwich *et al.* (9) showed that ovarian tumor initiating cells adhered to type IV collagen, but it was not clear if these were derived from FTE. The cell of origin may be important when considering factors that enhance ovarian colonization, such as increased WNT4 expression detected after loss of PTEN in fallopian-tube-derived tumor cell lines (16). All together, these investigations suggest a model where in women the ovary produces chemoattractant factors that draw FTE cells to the ovary, which then allows FTE cells to bind to the exposed ECM during and after ovulation.

We have shown previously that PTEN^{shRNA}, but not AKT^{myr}, confers tumorigenic properties to MOE cells (15). Here, multiple pathway alterations that are associated with HGSOC (p53 mutation, activation of KRAS, loss of PTEN) were tested; however, only loss of PTEN reversed the low 3D:2D viability ratio seen in normal MOE cells on 3D collagen. PTEN loss also increased attachment, invasion and spheroid formation, suggesting that loss of PTEN is sufficient to drive colonization of the ovary, which was supported by a transgenic mouse model (16). In both The Cancer Genome Atlas datasets for ovarian cancer, PTEN is genetically deleted in less than 7% of HGSOC cases (13). However, a recent study using whole-exome sequencing of laser-capture microdissections found that five of nine STICs had a loss of PTEN or a somatic mutation in the gene (2). Immunohistochemistry of STICs found 33% to be negative for PTEN (33), and Martins *et al.* (34) found that PTEN protein was low or absent in the tumor cells in over 50% of HGSOC cases. Multiple microRNAs that target PTEN have been shown to be overexpressed in ovarian cancer (35,36), suggesting posttranscriptional mechanisms also contribute to loss of PTEN. Collectively, these results suggest that loss of PTEN may be more frequent than appreciated in HGSOC derived from FTE due to mechanisms that control PTEN expression beyond genetic loss.

Loss of PTEN or activation of PI3K is common across multiple types of cancer (29,37,38). Historically, the importance of these signaling alterations was attributed to activation of AKT. However, it is becoming increasingly clear that PTEN loss activates multiple pathways that are required for transformation. Transcriptomic analysis in A431 (epidermoid carcinoma), HCC827 (non-small-cell lung carcinoma) and SKBR-3 (mammary adenocarcinoma) cells with and without PTEN deletion identified increased JNK signaling (29). Importantly, this increase was mediated by RAC1 and was AKT independent. In agreement, restoration of PTEN in glioblastoma reduced phospho-JNK levels (38). In this study, AKT and RAC1/JNK signaling contributed to the increased invasion seen in MOE PTEN^{shRNA} cells, whereas RAC1/JNK increased adhesion. Interestingly, results from experiments using MOE PTEN^{shRNA}, MOE AKT^{myr} and the AKT inhibitor MK2206 suggest that AKT activation contributes to, but is not sufficient for, increased 3D:2D viability. Inhibition of the RAC1/JNK pathway did not reverse the phenotype seen in MOE PTEN^{shRNA} cells.

In this study, we used MOE cells due to their known tissue of origin and our collection of stable clones that mimic changes common in HGSOC (15,20). We also used OVCAR8 cells due to their mutation in p53 (39), their ability to form aggressive tumors *in vivo* (40) and their classification as possibly HGSOC based on genetic analysis (41). However, it is possible that cancer cells propagated on plastic have acquired behavior that affects their response. Patient-derived xenografts were originally proposed to model *in situ* cancers from patients, but even those have recently been shown to evolve away from the original tumors (42). Therefore, primary cells would be a better model system, but many of the assays required GFP or RFP expression, necessitating at least short-term growth on plastic and clonal selection. Finally, primary normal FTE cells would not allow us to investigate genetic changes common in HGSOC whereas primary cells from HGSOC tumors would contain many mutations, making it challenging to investigate the effect of specific mutations.

In conclusion, tumorigenic FTE cells grafted in the bursa colonized the ovary and then metastasized throughout the peritoneum. FTE cells preferentially bound to ECM, particularly collagen, found under the OSE; however, the viability of normal FTE cells was reduced by 3D type I collagen. Loss of PTEN activated phospho-AKT and RAC1/JNK, which led to increased cell viability on 3D collagen, increased attachment of FTE cells to ovaries and increased invasion through 3D collagen. These results suggest that loss of PTEN may be an important step in metastasis from the fallopian tube to the ovary and the colonization of the ovary is a critical step in progression of HGSOC.

Supplementary material

Supplementary data are available at *Carcinogenesis* online.

Funding

Department of Defense (Grant OC130046); the Ovarian Cancer Research Fund Alliance Ann and Sol Schreiber Mentored Investigator Award (No. 543296); UG3 (ES029073).

Conflict of Interest Statement: The authors have no conflict of interest to declare.

References

1. Marquez, R.T. *et al.* (2005) Patterns of gene expression in different histotypes of epithelial ovarian cancer correlate with those in normal fallopian tube, endometrium, and colon. Clin. Cancer Res., 11, 6116–6126.
2. Labidi-Galy, S.I. *et al.* (2017) High grade serous ovarian carcinomas originate in the fallopian tube. Nat. Commun., 8, 1093.
3. Coscia, F. *et al.* (2016) Integrative proteomic profiling of ovarian cancer cell lines reveals precursor cell associated proteins and functional status. Nat. Commun., 7, 12645.
4. Falconer, H. *et al.* (2015) Ovarian cancer risk after salpingectomy: a nationwide population-based study. J. Natl. Cancer Inst., 107, dju410.
5. Hankinson, S.E. *et al.* (1993) Tubal ligation, hysterectomy, and risk of ovarian cancer. A prospective study. JAMA, 270, 2813–2818.
6. Samimi, G. *et al.* (2017) Opportunistic salpingectomy: what about the role of the ovary in ovarian cancer? Cancer, 123, 1699–1702.
7. Merritt, M.A. *et al.* (2013) Reproductive characteristics in relation to ovarian cancer risk by histologic pathways. Hum. Reprod., 28, 1406–1417.
8. Titus-Ernstoff, L. *et al.* (2001) Menstrual and reproductive factors in relation to ovarian cancer risk. Br. J. Cancer, 84, 714–721.
9. Yang-Hartwich, Y. *et al.* (2014) Ovulation and extra-ovarian origin of ovarian cancer. Sci. Rep., 4, 6116.
10. Wright, J.W. *et al.* (2010) Ovulation in the absence of the ovarian surface epithelium in the primate. Biol. Reprod., 82, 599–605.
11. Wright, J.W. *et al.* (2011) Dynamics of the primate ovarian surface epithelium during the ovulatory menstrual cycle. Hum. Reprod., 26, 1408–1421.
12. Dean, M. *et al.* (2017) Activin A stimulates migration of the fallopian tube epithelium, an origin of high-grade serous ovarian cancer, through non-canonical signaling. Cancer Lett., 391, 114–124.
13. Cancer Genome Atlas Research Network. (2011) Integrated genomic analyses of ovarian carcinoma. Nature, 474, 609–615.
14. Hanrahan, A.J. *et al.* (2012) Genomic complexity and AKT dependence in serous ovarian cancer. Cancer Discov., 2, 56–67.
15. Eddie, S.L. *et al.* (2015) Tumorigenesis and peritoneal colonization from fallopian tube epithelium. Oncotarget, 6, 20500–20512.
16. Russo, A. *et al.* (2018) PTEN loss in the fallopian tube induces hyperplasia and ovarian tumor formation. Oncogene, 37, 1976–1990.
17. Rodgers, L.H. *et al.* (2016) Loss of PAX8 in high-grade serous ovarian cancer reduces cell survival despite unique modes of action in the fallopian tube and ovarian surface epithelium. Oncotarget, 7, 32785–32795.
18. Moyle-Heyrman, G. *et al.* (2016) Genome-wide transcriptional regulation of estrogen receptor targets in fallopian tube cells and the role of selective estrogen receptor modulators. J. Ovarian Res., 9, 5.
19. Karthikeyan, S. *et al.* (2016) Cadherin-6 type 2, K-cadherin (CDH6) is regulated by mutant p53 in the fallopian tube but is not expressed in the ovarian surface. Oncotarget, 7, 69871–69882.
20. Quartuccio, S.M. *et al.* (2015) Mutant p53 expression in fallopian tube epithelium drives cell migration. Int. J. Cancer, 137, 1528–1538.
21. Barbolina, M.V. *et al.* (2009) Downregulation of connective tissue growth factor by three-dimensional matrix enhances ovarian carcinoma cell invasion. Int. J. Cancer, 125, 816–825.
22. Coffman, L.G. *et al.* (2016) New models of hematogenous ovarian cancer metastasis demonstrate preferential spread to the ovary and a requirement for the ovary for abdominal dissemination. Transl. Res., 175, 92–102.e2.
23. Nikulenkov, F. *et al.* (2012) Insights into p53 transcriptional function via genome-wide chromatin occupancy and gene expression analysis. Cell Death Differ., 19, 1992–2002.
24. Xia, H. *et al.* (2004) Focal adhesion kinase is upstream of phosphatidylinositol 3-kinase/Akt in regulating fibroblast survival in response to contraction of type I collagen matrices via a beta 1 integrin viability signaling pathway. J. Biol. Chem., 279, 33024–33034.
25. Levental, K.R. *et al.* (2009) Matrix crosslinking forces tumor progression by enhancing integrin signaling. Cell, 139, 891–906.
26. Vasudevan, K.M. *et al.* (2009) AKT-independent signaling downstream of oncogenic PIK3CA mutations in human cancer. Cancer Cell, 16, 21–32.
27. Nho, R.S. *et al.* (2005) Role of integrin-linked kinase in regulating phosphorylation of Akt and fibroblast survival in type I collagen matrices through a beta1 integrin viability signaling pathway. J. Biol. Chem., 280, 26630–26639.
28. Orlacchio, A. *et al.* (2017) SGK1 is a critical component of an AKT-independent pathway essential for PI3K-mediated tumor development and maintenance. Cancer Res., 77, 6914–6926.
29. Vivanco, I. *et al.* (2007) Identification of the JNK signaling pathway as a functional target of the tumor suppressor PTEN. Cancer Cell, 11, 555–569.
30. Liliental, J. *et al.* (2000) Genetic deletion of the Pten tumor suppressor gene promotes cell motility by activation of Rac1 and Cdc42 GTPases. Curr. Biol., 10, 401–404.
31. Mense, S.M. *et al.* (2015) PTEN inhibits PREX2-catalyzed activation of RAC1 to restrain tumor cell invasion. Sci. Signal., 8, ra32.
32. Perets, R. *et al.* (2013) Transformation of the fallopian tube secretory epithelium leads to high-grade serous ovarian cancer in Brca;Tp53;Pten models. Cancer Cell, 24, 751–765.
33. Roh, M.H. *et al.* (2010) High-grade fimbrial-ovarian carcinomas are unified by altered p53, PTEN and PAX2 expression. Mod. Pathol., 23, 1316–1324.
34. Martins, F.C. *et al.* (2014) Combined image and genomic analysis of high-grade serous ovarian cancer reveals PTEN loss as a common driver event and prognostic classifier. Genome Biol., 15, 526.
35. Yang, H. *et al.* (2008) MicroRNA expression profiling in human ovarian cancer: miR-214 induces cell survival and cisplatin resistance by targeting PTEN. Cancer Res., 68, 425–433.
36. Lou, Y. *et al.* (2010) MicroRNA-21 promotes the cell proliferation, invasion and migration abilities in ovarian epithelial carcinomas through inhibiting the expression of PTEN protein. Int. J. Mol. Med., 26, 819–827.
37. Thorpe, L.M. *et al.* (2015) PI3K in cancer: divergent roles of isoforms, modes of activation and therapeutic targeting. Nat. Rev. Cancer, 15, 7–24.
38. Rong, Y. *et al.* (2009) Epidermal growth factor receptor and PTEN modulate tissue factor expression in glioblastoma through JunD/activator protein-1 transcriptional activity. Cancer Res., 69, 2540–2549.
39. Leroy, B. *et al.* (2014) Analysis of TP53 mutation status in human cancer cell lines: a reassessment. Hum. Mutat., 35, 756–765.
40. Mitra, A.K. *et al.* (2015) *In vivo* tumor growth of high-grade serous ovarian cancer cell lines. Gynecol. Oncol., 138, 372–377.
41. Domcke, S. *et al.* (2013) Evaluating cell lines as tumour models by comparison of genomic profiles. Nat. Commun., 4, 2126.
42. Ben-David, U. *et al.* (2017) Patient-derived xenografts undergo mouse-specific tumor evolution. Nat. Genet., 49, 1567–1575.